AIAA 2004-4082

Simulation of 3D Flows of Propulsion Systems Using an Efficient Low Diffusion E-CUSP Upwind Scheme

Zongjun Hu and Gecheng Zha
Department of Mechanical and Aerospace Engineering, University of Miami, Coral Gables, FL 33124

40th AIAA/ASME/SAE/ASEE Joint Propulsion Conference and Exhibit July 11-14, Fort Lauderdale, Florida

For permission to copy or republish, contact the American Institute of Aeronautics and Astronautics 1801 Alexander Bell Drive, Suite 500, Reston, VA 20191–4344

Simulation of 3D Flows of Propulsion Systems Using an Efficient Low Diffusion E-CUSP Upwind Scheme

Zongjun Hu* and Gecheng Zha†
Department of Mechanical and Aerospace Engineering, University of Miami, Coral Gables, FL 33124

Abstract

A newly suggested E-CUSP upwind scheme is employed for the first time to calculate 3D flows of propulsion systems. The computed cases include a transonic nozzle with circular-to-rectangular cross section, a transonic duct with shock wave/turbulent boundary layer interaction, and a subsonic 3D compressor cascade. The computed results agree well with the experiments. The new scheme is proved to be accurate, efficient and robust for the 3D calculations of the flows in this paper.

Introduction

The aircraft engine propulsion systems usually work in transonic regime, where the resolution of shock waves and boundary layers are very important. The 3D flow field calculation is usually CPU intensive. Hence, an accurate and efficient Riemann solver to resolve the shock waves and boundary layer is necessary.

The well known Roe scheme[1] is accurate to resolve the shock waves and boundary layer. However, the Roe scheme needs matrix operation for its numerical dissipation, which is fairly CPU intensive. Recently, there are many efforts to develop efficient Riemann solvers using scalar dissipation instead of the matrix dissipation. For the scalar dissipation Riemann solver schemes, there are generally two types: H-CUSP schemes and E-CUSP schemes.[2–4] The abbreviation CUSP stands for "convective upwind and split pressure" named by Jameson.[2–4] The H-CUSP schemes have the total enthalpy from the energy equation in their convective vectors, while the E-CUSP schemes use the total energy in the convective vectors. The Liou's AUSM family schemes, Van Leer-Hänel scheme,[5] and Edwards's LDFSS schemes[6,7] belong to the H-CUSP group.

The H-CUSP schemes may have the advantages to better conserve the total enthalpy for steady state flows. However, from the characteristic theory point of view, the H-CUSP schemes are not fully consistent with the disturbance propagation directions, which may affect the stability and robustness of the schemes.[8] A H-CUSP scheme may have more inconsistency when it is extended to moving grid system. It will leave a pressure term multiplied by the grid velocity in the energy flux that is not contained in the total enthalpy and the term will be treated as a part of the pressure term. From characteristics point of view, it is not obvious how to treat this term in a consistent manner.[9]

Recently, Zha and Hu suggested an efficient E-CUSP scheme (named as Zha CUSP) which is consistent with the characteristic directions.[8] The scheme has low diffusion and is able to capture crisp shock profiles and exact contact discontinuities. The scheme is shown to be accurate, robust and efficient. In addition, it is straightforward to extend the Zha CUSP scheme to moving grid system.[9]

The original E-CUSP scheme of Zha and Hu is further modified to remove the temperature oscillations occurring occasionally near walls, in particular when the mesh is skewed.[10] Zha modified the scheme by replacing the pressure in the dissipation of energy equation with the total enthalpy.[10] The modified scheme also yields more precise wall surface temperature at coarse grid.[10] The modified scheme is named Zha CUSP2 scheme. Neither the original Zha CUSP scheme nor the Zha CUSP2 scheme has ever been applied to 3D flow field calculations.

This paper is to extend and apply the Zha CUSP2 scheme to 3D calculation of internal flows of propulsion systems. The scheme is demonstrated to be accurate, efficient, and robust for the 3D flows calculated in this paper.

Governing Equations

The governing equations are the 3D Reynolds averaged Navier-Stokes equations in conservation law form and in generalized coordinates, and is given as,

$$\begin{aligned}&\frac{\partial \boldsymbol{Q}}{\partial t}+\frac{\partial \boldsymbol{E}}{\partial \xi}+\frac{\partial \boldsymbol{F}}{\partial \eta}+\frac{\partial \boldsymbol{G}}{\partial \zeta}\\&=\frac{1}{Re}\left(\frac{\partial \boldsymbol{R}}{\partial \xi}+\frac{\partial \boldsymbol{S}}{\partial \eta}+\frac{\partial \boldsymbol{T}}{\partial \zeta}\right)\end{aligned} \tag{1}$$

where $\boldsymbol{Q}$ is the conservative variable vector, $\boldsymbol{E}$, $\boldsymbol{F}$, $\boldsymbol{G}$ and $\boldsymbol{R}$, $\boldsymbol{S}$, $\boldsymbol{T}$ are the inviscid and viscous flux vectors in ξ, η, ζ directions respectively.

To save space, only the contents of $\boldsymbol{Q}$, and fluxes in ξ direction, $\boldsymbol{E}$ and $\boldsymbol{R}$ are given below.

$$\boldsymbol{Q}=\frac{1}{J}\begin{pmatrix}\rho\\ \rho u\\ \rho v\\ \rho w\\ \rho e\end{pmatrix} \tag{2}$$

*Phd Student

†Associate Professor, Director of CFD lab

Copyright © 2004 by Zongjun Hu and Gecheng Zha. Published by the American Institute of Aeronautics and Astronautics, Inc. with permission.

$$\boldsymbol{E} = \begin{pmatrix} \rho U \\ \rho u U + l_x p \\ \rho v U + l_y p \\ \rho w U + l_z p \\ (\rho e + p)\, U \end{pmatrix} \tag{3}$$

$$\boldsymbol{R} = \begin{pmatrix} 0 \\ l_x \tau_{xx} + l_y \tau_{xy} + l_z \tau_{xz} \\ l_x \tau_{xy} + l_y \tau_{yy} + l_z \tau_{yz} \\ l_x \tau_{xz} + l_y \tau_{yz} + l_z \tau_{zz} \\ l_x \beta_x + l_y \beta_y + l_z \beta_z \end{pmatrix} \tag{4}$$

where, J is the transformation Jacobian, ρ is the density, e is the total energy per unit mass, u, v, w are the velocity components in x, y, z direction. The static pressure p is determined as,

$$p = (\gamma - 1)\left[\rho e - \frac{1}{2}\rho\left(u^2 + v^2 + w^2\right)\right] \tag{5}$$

U is the normal contravariant velocity in generalized ξ direction,

$$U = \boldsymbol{V} \cdot \boldsymbol{l} = u l_x + v l_y + w l_z \tag{6}$$

The vector $\boldsymbol{l}$ is the control volume interface area vector pointing in the direction normal to the interface with its magnitude equal to the interface area. When $\Delta\xi = \Delta\eta = \Delta\zeta = 1$, $\boldsymbol{l}$ is expressed as the following,

$$\boldsymbol{l} = l_x \boldsymbol{i} + l_y \boldsymbol{j} + l_z \boldsymbol{k} = \frac{1}{J}\left(\xi_x \boldsymbol{i} + \xi_y \boldsymbol{j} + \xi_z \boldsymbol{k}\right) \tag{7}$$

Shear stress components, τ_{xx}, τ_{xy}, τ_{xz}, τ_{yy}, τ_{yz}, τ_{zz} are defined as,

$$\begin{aligned} \tau_{ij} \quad = \quad & -\frac{2}{3}\left(\mu + \mu_t\right)\frac{\partial u_k}{\partial x_k}\delta_{ij} \\ & + \left(\mu + \mu_t\right)\left(\frac{\partial u_i}{\partial x_j} + \frac{\partial u_j}{\partial x_i}\right) \end{aligned} \tag{8}$$

where, μ is the molecular viscosity, μ_t is the turbulent viscosity.

β_x, β_y, β_z are defined as,

$$\beta_i = u_j \tau_{ij} - q_i \tag{9}$$

where, q_x, q_y, $q_z$are the heat fluxes in x, y, z direction.

$$\bar{q_i} = -\left[\frac{\bar{\mu}}{(\gamma - 1)\,\mathrm{Pr}} + \frac{\bar{\mu}_t}{(\gamma - 1)\,\mathrm{Pr}_t}\right]\frac{\partial a^2}{\partial x_i} \tag{10}$$

Where, Pr and Pr_t are the molecular and turbulence Prandtl number taken the value of 0.72 and 0.9. The turbulence viscosity is calculated using Baldwin-Lomax turbulence model.[11] a is the speed of sound.

The control volume method is used to discretize the governing equations on mesh cell $(i,\, j,\, k)$ as:

$$\begin{aligned} & \frac{\partial}{\partial t}\int_{\mathrm{d}V_{i,j,k}} \boldsymbol{Q}\,\mathrm{d}\xi\mathrm{d}\eta\mathrm{d}\zeta + \left(\boldsymbol{E}_{i+\frac{1}{2}} - \boldsymbol{E}_{i-\frac{1}{2}}\right) \\ & + \left(\boldsymbol{F}_{j+\frac{1}{2}} - \boldsymbol{F}_{j-\frac{1}{2}}\right) + \left(\boldsymbol{G}_{k+\frac{1}{2}} - \boldsymbol{G}_{k-\frac{1}{2}}\right) \\ & = \frac{1}{\mathrm{Re}}\left[\left(\boldsymbol{R}_{i+\frac{1}{2}} - \boldsymbol{R}_{i-\frac{1}{2}}\right) + \left(\boldsymbol{S}_{j+\frac{1}{2}} - \boldsymbol{S}_{j-\frac{1}{2}}\right)\right. \\ & \left. + \left(\boldsymbol{T}_{k+\frac{1}{2}} - \boldsymbol{T}_{k-\frac{1}{2}}\right)\right] \end{aligned} \tag{11}$$

where $i \pm \frac{1}{2}$, $j \pm \frac{1}{2}$ and $k \pm \frac{1}{2}$ represent the control volume left and right interface locations in ξ, η and ζ directions.

The E-CUSP Scheme (Zha CUSP2)

Take ξ direction as example, the original Zha CUSP scheme splits the inviscid flux $\boldsymbol{E}$ on interface $i \pm \frac{1}{2}$ into convective vector $\boldsymbol{E}^c$ and wave vector $\boldsymbol{E}^p$ to represent the velocity and pressure wave characteristics.[8] The total energy is included in the convective vector. In subsonic regime, the convective vector $\boldsymbol{E}^c$ is treated in an upwind manner, and the pressure vector $\boldsymbol{E}^p$ is averaged with the weight of the eigenvalues $U \pm C$ from both the upwind and the downwind directions. C is the speed of sound multiplied by the interface area:

$$C = a\sqrt{l_x^2 + l_y^2 + l_z^2} \tag{12}$$

where $a = \sqrt{\gamma RT}$ is the speed of sound
The interface flux $\boldsymbol{E}_{\frac{1}{2}}$ is evaluated as the following.

1. In subsonic region, $|U|_{\frac{1}{2}} < C_{\frac{1}{2}}$,

$$\begin{aligned} \boldsymbol{E}_{\frac{1}{2}} = & \frac{1}{2}\left[(\rho U)_{\frac{1}{2}}\left(\boldsymbol{q}_L^c + \boldsymbol{q}_R^c\right) - |\rho U|_{\frac{1}{2}}\left(\boldsymbol{q}_R^c - \boldsymbol{q}_L^c\right)\right] \\ & + \frac{1}{2}\begin{pmatrix} 0 \\ \mathcal{P}^+ p\, l_x \\ \mathcal{P}^+ p\, l_y \\ \mathcal{P}^+ p\, l_z \\ \frac{1}{2}p\left[U + C_{\frac{1}{2}}\right] \end{pmatrix}_L + \begin{pmatrix} 0 \\ \mathcal{P}^- p\, l_x \\ \mathcal{P}^- p\, l_y \\ \mathcal{P}^- p\, l_z \\ \frac{1}{2}p\left[U - C_{\frac{1}{2}}\right] \end{pmatrix}_R \end{aligned} \tag{13}$$

where,

$$\boldsymbol{q}^c = \begin{pmatrix} 1 \\ u \\ v \\ w \\ e \end{pmatrix} \tag{14}$$

The subscripts L and R represent the left and right hand sides of the interface. The interface speed of sound $C_{\frac{1}{2}}$ is computed as,

$$C_{\frac{1}{2}} = \frac{1}{2}\left(C_L + C_R\right) \tag{15}$$

where C_L and C_R are the speed of sound determined from the left and the right side of the interface.

The mass flux on the interface is introduced as the following,

$$(\rho U)_{\frac{1}{2}} = \left(\rho_L U_L^+ + \rho_R U_R^-\right) \tag{16}$$

where,

$$U_L^+ = C_{\frac{1}{2}} \left\{ \frac{M_L+|M_L|}{2} + \alpha_L \left[\frac{1}{4}\left(M_L+1\right)^2 - \left(\frac{M_L+|M_L|}{2} \right) \right] \right\} \tag{17}$$

$$U_R^- = C_{\frac{1}{2}} \left\{ \frac{M_R-|M_R|}{2} + \alpha_R \left[-\frac{1}{4}\left(M_R-1\right)^2 - \left(\frac{M_R-|M_R|}{2} \right) \right] \right\} \tag{18}$$

$$\alpha_L = \frac{2\left(p/\rho\right)_L}{\left(p/\rho\right)_L + \left(p/\rho\right)_R} \tag{19}$$

$$\alpha_R = \frac{2\left(p/\rho\right)_R}{\left(p/\rho\right)_L + \left(p/\rho\right)_R} \tag{20}$$

$$M_L = \frac{U_L}{C_{\frac{1}{2}}} \tag{21}$$

$$M_R = \frac{U_R}{C_{\frac{1}{2}}} \tag{22}$$

The coefficient $\mathcal{P}$ is defined as,

$$\mathcal{P}_L^+ = \frac{1}{4}\left(M_L+1\right)^2\left(2-M_L\right) + \alpha M_L \left(M_L^2-1\right)^2 \tag{23}$$

$$\mathcal{P}_R^- = \frac{1}{4}\left(M_R-1\right)^2\left(2+M_R\right) - \alpha M_R \left(M_R^2-1\right)^2 \tag{24}$$

where

$$\alpha = \frac{3}{16}$$

2. In supersonic region, $|U|_{\frac{1}{2}} \geqslant C_{\frac{1}{2}}$, $\boldsymbol{E}_{\frac{1}{2}}$ is simply computed using upwind variables.

   When $U_{\frac{1}{2}} > C_{\frac{1}{2}}$,

$$\boldsymbol{E}_{\frac{1}{2}} = \boldsymbol{E}_L \tag{25}$$

   When $U_{\frac{1}{2}} < -C_{\frac{1}{2}}$,

$$\boldsymbol{E}_{\frac{1}{2}} = \boldsymbol{E}_R \tag{26}$$

The above formulations are for the original Zha CUSP scheme, which can capture sharp shock profiles and exact contact surface with low diffusion.[8] However, the scheme is found to have temperature oscillations near the wall when the grid is skewed. The Zha CUSP scheme is hence modified to the following Zha CUSP2 scheme:[10]

The total enthalpy instead of the static pressure is used to compute the numerical dissipation coefficients α_L and α_R for the energy equation,

$$\alpha_L = \frac{2\left(H/\rho\right)_L}{\left(H/\rho\right)_L + \left(H/\rho\right)_R} \tag{27}$$

$$\alpha_R = \frac{2\left(H/\rho\right)_R}{\left(H/\rho\right)_L + \left(H/\rho\right)_R} \tag{28}$$

The total enthalpy is calculated as,

$$H = e + \frac{p}{\rho} \tag{29}$$

It needs to emphasize that, when computing the fluxes of continuity and momentum equations, the formulations of the α_L and α_R given in Eq. (19) and Eq. (20) must be used. Eq.(27) and (28) are only for the energy equation.

The temperature oscillations are removed by using eq.(27) and (28) and the wall temperature is more precisely predicted by this modified scheme if a coarse grid is used.[10] This modified scheme is used for the computations in this paper.

Turbulence Model

The turbulent viscosity μ_t is computed based on Baldwin-Lomax two-layer algebraic model.[11] At inner layer,

$$\mu_{ti} = \rho l^2 \left|\omega\right| \tag{30}$$

where

$$l = ky\left[1-\exp\left(-\frac{y^+}{A^+}\right)\right] \tag{31}$$

ω is the local vorticity, y and y^+ are the dimensional and dimensionless distance to the wall.

At the outer layer,

$$\mu_{to} = KC_{\mathrm{cp}}\rho F_{\mathrm{wake}} F_{\mathrm{kleb}} \tag{32}$$

$$F_{\mathrm{wake}} = \min\left(y_{\max}F_{\max},\, C_{\mathrm{wake}}y_{\max}u_{\mathrm{diff}}^2/F_{\max}\right)$$

$$F_{\mathrm{kleb}} = \left[1+5.5\left(\frac{C_{\mathrm{kleb}}y}{y_{\max}}\right)^6\right]^{-1}$$

In the above formulations, k, A^+, C_{wake}, C_{kleb}, C_{cp} and K are constants.

The quantities u_{diff}, $F_{\max}$ and $y_{\max}$ are determined by the velocity profile following a line normal to the wall. $F_{\max}$ and $y_{\max}$ are the maximum value and the corresponding distance of function F_y,

$$F_y = y\,|\omega|\left[1-\exp\left(-\frac{y^+}{A^+}\right)\right] \tag{33}$$

$$u_{\text{diff}} = \left(\sqrt{u^2+v^2+w^2}\right)_{\max} - \left(\sqrt{u^2+v^2+w^2}\right)_{\min} \tag{34}$$

In the 3D computation of this paper, the wall is located at the 4 side of the computation domain. The value of μ_t is simply computed according to the closest wall surface. $F_{\max}$ and $y_{\max}$ is searched from the wall to the center of the passage. In the wake region, the exponential part is set to zero in Eq. (31) and Eq. (33). The second part of Eq. (34) is set to be zero outside of the wake region.

Time Marching Method

The linearized governing equation, Eq. (11), is solved implicitly using the line *Gauss-Seidel* iteration method. The iteration is swept line by line in the vertical η direction within each time step. The updated variables are used immediately in the previous neighboring line during the sweep as the Gauss-Seidel iteration requires. Two alternating direction sweeps are used in each time step with one sweep from *inlet* to *outlet*, and the other from *outlet* to *inlet*. First order Euler scheme is used to discretize the temporal term. First order scheme discretization in space is also used for the implicit left hand side operator to enhance the diagonal dominance.

The discretized implicit equations is given as the following:

$$\begin{aligned} I\Delta\boldsymbol{Q}_{i,j,k} &+ A^+\Delta\boldsymbol{Q}_{i+1,j,k} + A\Delta\boldsymbol{Q}_{i,j,k} \\ &+ A^-\Delta\boldsymbol{Q}_{i-1,j,k} + B^+\Delta\boldsymbol{Q}_{i,j+1,k} \\ &+ B\Delta\boldsymbol{Q}_{i,j,k} + B^-\Delta\boldsymbol{Q}_{i,j-1,k} \\ &+ C^+\Delta\boldsymbol{Q}_{i,j,k+1} + C\Delta\boldsymbol{Q}_{i,j,k} \\ &+ C^-\Delta\boldsymbol{Q}_{i,j,k-1} \\ &= \boldsymbol{RHS} \end{aligned} \tag{35}$$

where,

$$\Delta\boldsymbol{Q} = \boldsymbol{Q}^{n+1} - \boldsymbol{Q}^n$$

$$\begin{aligned} \boldsymbol{RHS} = \frac{\Delta t}{\Delta V}\Bigg\{ & \frac{1}{Re}\Big[\Big(\boldsymbol{R}_{i+\frac{1}{2}} - \boldsymbol{R}_{i-\frac{1}{2}}\Big) \\ & + \Big(\boldsymbol{S}_{j+\frac{1}{2}} - \boldsymbol{S}_{j-\frac{1}{2}}\Big) + \Big(\boldsymbol{T}_{k+\frac{1}{2}} - \boldsymbol{T}_{k-\frac{1}{2}}\Big)\Big] \\ & - \Big[\Big(\boldsymbol{E}_{i+\frac{1}{2}} - \boldsymbol{E}_{i-\frac{1}{2}}\Big) + \Big(\boldsymbol{F}_{j+\frac{1}{2}} - \boldsymbol{F}_{j-\frac{1}{2}}\Big) \\ & + \Big(\boldsymbol{G}_{k+\frac{1}{2}} - \boldsymbol{G}_{k-\frac{1}{2}}\Big)\Big]\Bigg\}^n \end{aligned} \tag{36}$$

The superscripts n and $n+1$ denote two sequential time steps. A, B, C, A^+, B^+, C^+, A^-, B^-, $C^-$are derived Jacobian coefficient matrices. I is the identity matrix of order 5. The van Leer scheme[12] is used to construct the Jacobians for its diagonal dominance nature.

The equation system is rewritten into the following form for η-direction line *Gauss-Seidel* iteration.

$$\begin{aligned} B^-\Delta\boldsymbol{U}_{i,j-1,k} + \overline{B}\Delta\boldsymbol{U}_{i,j,k} + B^+\Delta\boldsymbol{U}_{i,j+1,k} \\ = \boldsymbol{RHS}^* \end{aligned} \tag{37}$$

where

$$\overline{B} = I + A + B + C \tag{38}$$

$$\begin{aligned} \boldsymbol{RHS}^* = \boldsymbol{RHS} - A^+\Delta\boldsymbol{U}_{i+1,j,k} - A^-\Delta\boldsymbol{U}_{i-1,j,k} \\ -C^+\Delta\boldsymbol{U}_{i,j,k+1} - C^-\Delta\boldsymbol{U}_{i,j,k-1} \end{aligned} \tag{39}$$

Results and Discussion

The 3D Zha CUSP2 scheme is applied to subsonic and transonic 3D internal flow cases for validation. The cases include: 1) a transonic nozzle with circular-to-rectangular cross section; 2) a transonic channel flow with shock wave/turbulent boundary layer interaction; and 3) a subsonic compressor cascade. In the following computations, third order accuracy is used for the inviscid fluxes with MUSCL type differencing[13] and the Minmod limiter. Central-differencing is used for computing the viscous fluxes. The meshes are clustered in regions close to the wall, and the y^+ on the first inner mesh point is kept less than 3 on wall boundaries for all cases. Local time stepping is used to speed up the convergence.

Circular-to-rectangular Nozzle

A transonic nozzle with circular-to-rectangular cross section tested at NASA[14] is calculated. The transition duct connects the axisymmetric engine to the nonaxisymmetric nozzle through a smooth progression of geometrically similar cross sections. There is no swirl flow at the inlet. The Reynolds number is Re=$1.522\times10^5/in$. Due to its symmetric structure, only a quarter of the nozzle geometry is computed as shown in Fig. 1. Two symmetric boundaries are located at the bottom and back sides. The wall is divide into two parts to generate the H-type mesh. For clarity, every two other grid line is omitted in each direction in the plot. The baseline mesh size is 100×50×50 and is highly stretched near the walls. No shock wave exists in the flow field. The total pressure, total temperature and flow angles are fixed at the inlet as the boundary conditions. Because of the supersonic flow at the outlet, zero-gradient boundary condition is used at the nozzle exit. No slip and adiabatic wall conditions are used for the walls. The optimum CFL number used is 200.

Fig. 2 shows the contour lines of Mach number on the bottom symmetric plane for Zha CUSP2 scheme. The flow accelerates from subsonic at the inlet, reaches sonic at the nozzle throat, and becomes supersonic at the exit. The top wall and side wall static pressure distributions are compared with experimental results in Fig. 3 and Fig. 4 respectively.

Good agreement is obtained. The pressure distributions of Zha CUSP2 scheme and Roe scheme are indistinguishable on both the top and the side walls.

Because Zha CUSP2 scheme uses scalar dissipation and hence is more CPU efficient than the Roe scheme. On an Intel Xeon 1.7G Hz processor, the CPU time used to compute the inviscid flux per step per node is 1.84×10^{-5}s for the Zha CUSP2 scheme and 2.9723×10^{-5}s for the Roe scheme . The Zha CUSP2 scheme is about 40 percent more efficient.

Mesh refinement study is carried out by doubling mesh density in ξ, η and ζ directions respectively. The computation results with mesh $200\times50\times50$, $100\times100\times50$ and $100\times50\times100$ are also plotted in Fig. 3 and Fig. 4. The same mesh height is kept on the first inner cell close to the wall boundary for the mesh refinement. The mesh refinement gives about the same results as the original baseline mesh as shown in Fig. 3 and 4, which indicate that the solution is converged based on the mesh refinement.

3D Compressor Cascade

The third case is to calculate a 3D subsonic compressor cascade tested at NASA GRC.[16] The cascade has the chord length of 8.89 cm, the stagger angle of 60° and the solidity of 1.52. In the experiment, the geometry incidence is set to 0°. However, due to the side wall boundary layer effect, the actual incidence angle is considered to be $1^\circ to 1.5^\circ$ higher. In the numerical simulation, the incidence angle is set as 1.5°. The Reynolds number based the chord length is 9.67×10^5. A mesh of $100\times60\times60$ is used in the computation (Fig. 5).

The simulation includes the top and bottom end walls, where the cascade airfoil shape is very different from the one in the midspan as shown in Fig. 6. The computation starts from zero initial velocity field. The total pressure, total temperature and flow angles are fixed at the inlet. The static pressure is specified at the outlet. No slip and adiabatic wall boundary conditions are applied on blade surfaces and top, bottom end walls. Periodic boundary conditions are applied upstream and downstream of the blade.

Fig. 7 shows the Mach number contours of Zha CUSP2 scheme on the mid-span plane. Fig. 8 shows that the computed surface pressure ($C_p = \frac{p-p_\infty}{\frac{1}{2}\rho_\infty U_\infty^2}$) distribution agrees very well with the experiment. The result of the Zha CUSP2 scheme is also virtually identical to that of the Roe scheme.

Transonic Channel Flow

The second case is the transonic channel flow with shock wave/turbulent boundary-layer interaction and is studied experimentally in.[15] The test section of the transonic channel has an entrance height of 100 mm and a width of 120 mm. It is composed of a straight top wall, two straight side walls. A bump with varying shape in span-wise direction is mounted on the bottom wall. The boundary conditions are to fix the total pressure, total temperature and flow angles at the inlet and static pressure at the outlet. No slip adiabatic wall boundary conditions are used on the walls.

In the present computation, the inlet Mach number is about 0.5. The Reynolds number based on the entrance height is 5×10^5. A mesh of $90\times60\times60$ is used for computation. The mesh is mostly uniformly distributed in horizontal direction, but clustered in the bump region to better resolve the shock wave. Fig. 9 shows the 3D mesh with every two other grid line omitted for clarity. To resolve the turbulent boundary layer, the mesh is clustered near the four walls.

Fig. 10 shows the computed shock wave structure (Mach number contour) compared with the experiment at 3 spanwise planes. They are located at 60 mm, 75 mm and 90 mm away from the back wall respectively. The plane at 60mm is the central plane of the channel. The outlet static pressure is adjusted to achieve the same shock location as that in the experiment. The back pressure has the value of $p_{outlet}/P_t = 0.53$. The Zha CUSP2 scheme and the Roe scheme result in the shock wave structure very similar to the experiment. The computed maximum Mach numbers using Roe and Zha CUSP scheme are a little lower than that in the experiment. However, the Zha CUSP2 scheme gives the maximum Mach number closer to the experiment than the Roe scheme. Both the schemes predict the boundary layer thicker than that measured in the experiment. This may be mainly due to the inadequacy of the turbulence modeling.

At Z =60 mm, the experiment shows no flow separation. The Zha CUSP2 scheme also yields the attached flow. The Roe scheme predicts a flow separation at that location, which is different from the experiment. At location Z =75mm, both the Zha CUSP2 scheme and the Roe scheme predict the flow separation similar to the experiment. However, at the location Z =90 mm which is close to the side wall, the results computed by both the schemes predict larger separation zone than that of the experiment.

The mesh refinement study with the mesh size of $180\times60\times60$, $90\times90\times60$ and $90\times60\times90$ gives very similar results, which indicates that the solution is mesh independent.

Conclusion

The newly suggested E-CUSP upwind scheme with scalar dissipation, Zha CUSP2 scheme, is applied for the first time to calculate the 3D flows for propulsion systems.

For the transonic nozzle with circular-to-rectangular cross section and the subsonic compressor cascade, the wall static pressure distributions computed by both the Zha CUSP2 scheme and the Roe scheme are in good agreement with the experiments. The CPU time to calculate the flux using the Zha CUSP2 scheme is about 40% more efficient than that used by the Roe scheme.

For the transonic channel case, the shock wave structure given by Zha CUSP2 scheme agrees well with the experiment. The result of Zha CUSP2 scheme agrees better with the experiment than the one predicted by the Roe scheme, which gives flow separation that does not exist in the experiment. The Zha CUSP2 scheme also predicts the peak

Mach number closer to the experiment than that of the Roe scheme.

The Zha CUSP2 scheme is shown to be accurate, efficient and robust for the 3D flows calculated in this paper.

Acknowledgment

This work is partially supported by AFOSR Grant F49620-03-1-0253 monitored by Dr. Fariba Fahroo.

References

[1]P. Roe. Approximate riemann solvers, parameter vectors, and difference schemes. *Journal of Compuational Physics*, 43:357–72, 1981.

[2]A. Jameson. Analysis and design of numerical schemes for gas dynamics I: Artifi cial diffusion, upwind biasing, limiters and their effect on accuracy and multigrid convergence in transonic and hypersonic fbw. AIAA Paper 93-3359, 7 1993.

[3]A. Jameson. Analysis and Design of Numerical Schemes for Gas Dynamics I: Artifi cial Diffusion, Upwind Biasing, Limiters and Their Effect on Accuracy and Multigrid Convergence in Transonic and Hypersonic Flow. *Journal of Computational Fluid Dynamics*, 4:171–218, 1995.

[4]A. Jameson. Analysis and Design of Numerical Schemes for Gas Dynamics II: Artifi cial Diffusion and Discrete Shock Structure. *Journal of Computational Fluid Dynamics*, 5:1–38, 1995.

[5]D. Hänel, R. Schwane, and G. Seider. On the accuracy of upwind schemes for the solution of the navier-stokes equations. AIAA Paper 87-1105 CP, 1987.

[6]J. R. Edwards. A low-diffusion flux-splitting scheme for navier-stokes calculations. AIAA Paper 95-1703-CP, 6 1995.

[7]J. R. Edwards. A low-diffusion flux-splitting scheme for navier-stokes calculations. *Computer & Fluids*, 6:635–659, 1997.

[8]Gecheng Zha and Zongjun Hu. Calculation of transonic internal fbws using an effi cient high resolution upwind scheme. *to be published in AIAA Journal*, 2004. AIAA Paper 2004-1097.

[9]Xiangying Chen, Gecheng Zha, and Zongjun Hu. Numerical simulation of fbw induced vibration based on fully coupled fluid-structural interations. submitted to 34th AIAA Fluid Dynamics Conference, 2004.

[10]Gecheng Zha. A low diffusion effi cient e-cusp upwind scheme for transonic fbws. AIAA Paper 2004-2707, Submitted to AIAA Journal, 34th AIAA Fluid Dynamics Conference, June 28 - July 1, 2004.

[11]B. S. Baldwin and H. Lomax. Thin layer approximation and algebraic model for separated turbulent fbws. *AIAA Paper 78-257*, 1978.

[12]B. van Leer. Flux-vector splitting for the Euler equations. *Lecture Note in Physics*, 170, 1982.

[13]B. Van Leer. Towards the ultimate convservative difference scheme, III. *Jouranl of Computational Physics*, 23:263–75, 1977.

[14]James R. Burley II, Linda S. Bangert, and John R. Carlson. Static investigation of circular-to-rectangular transition ducts for high-aspect-ratio nonaxisymmetric nozzles. NASA Technical Paper 2534, 1986.

[15]Jean M. Délery. Experimental investigation of turbulence properties in transonic shock/boundary-layer interaction. *AIAA Journal*, 21, 1983.

[16]Daniel H. Buffum, Vincent R. Capece, Aaron J. King, and Yehia M. EL-Aini. Oscillating cascade aerodynamics at large mean incidence. Technical Memorandum 107247, NASA, 1996.

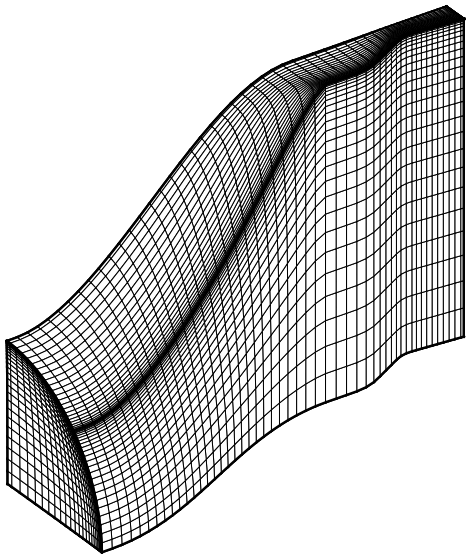

Fig. 1 The mesh of the nozzle with circular-to-rectangular cross section

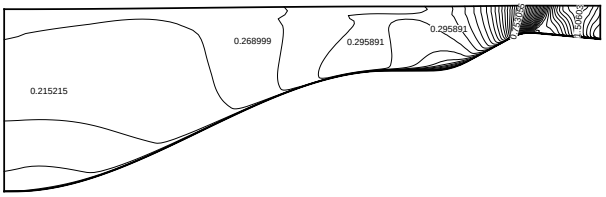

Fig. 2 Mach number contours of the nozzle with circular-to-rectangular cross section

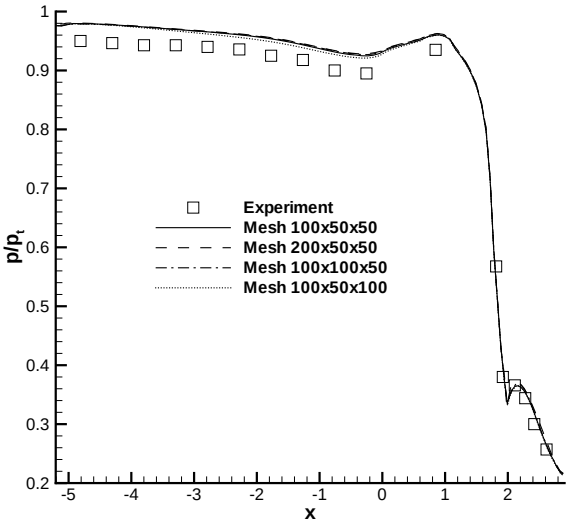

Fig. 3 Top wall surface pressure distributions of the nozzle with circular-to-rectangular cross section

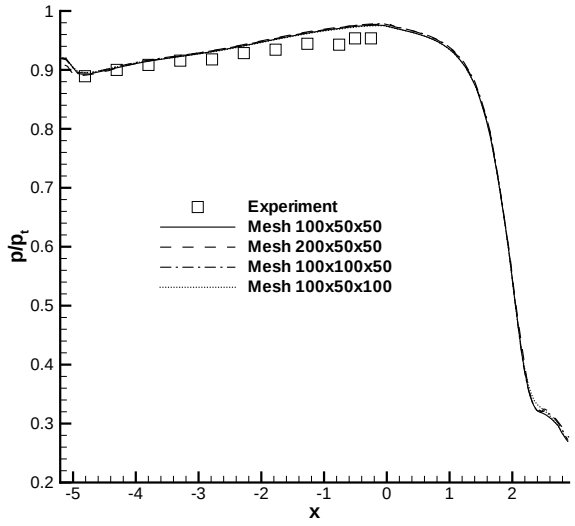

Fig. 4 Side wall surface pressure distributions of the nozzle with circular-to-rectangular cross section

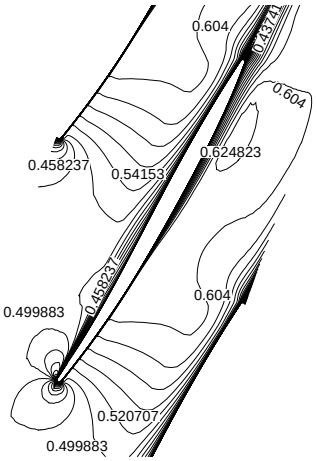

Fig. 7 Cascade Mach contours on the midspan plane

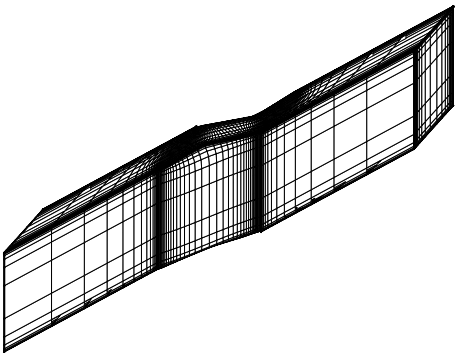

Fig. 5 3D cascade mesh

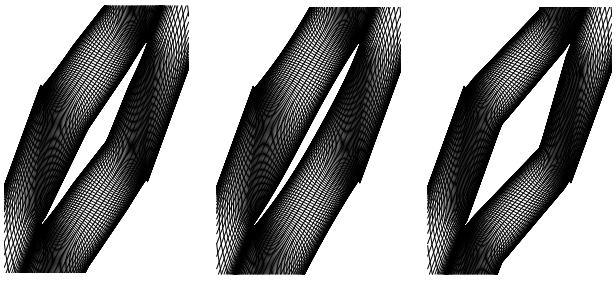

Fig. 6 Cascade Mesh on the bottom plane (left), midspan (middle), and top plane (right)

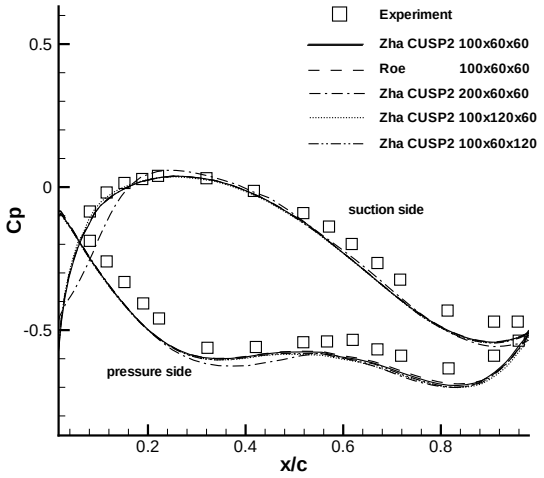

Fig. 8 Cascade midspan plane surface pressure coefficient distributions

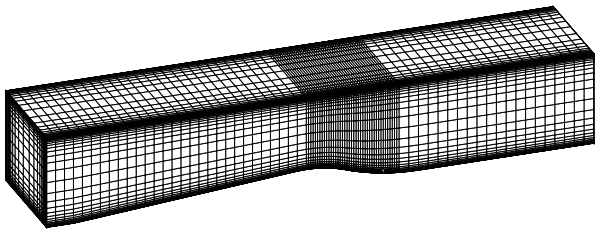

Fig. 9 Transonic duct mesh

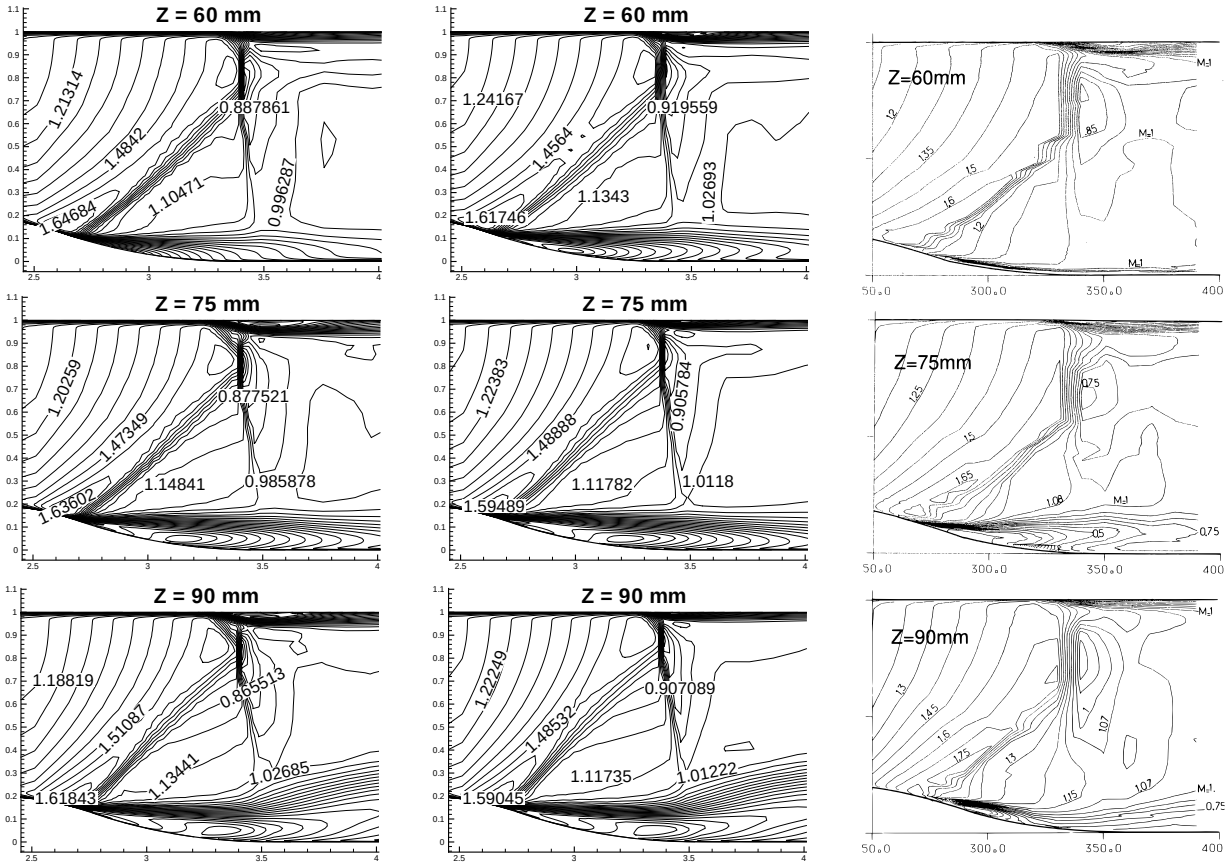

(A) Zha CUSP 2 scheme (B) Roe scheme (C) Experiment

Fig. 10 Transonic duct Mach number contours